Thermodynamic Stability of Annexin V E17G: Equilibrium Parameters from an Irreversible Unfolding Reaction[†,‡]

Thomas Vogl, Claudia Jatzke, and Hans-Jürgen Hinz*

Institut für Physikalische Chemie, Westfälische Wilhelms-Universität Münster, Schlossplatz 4/7, 48149 Münster, Germany

Jörg Benz and Robert Huber

Max-Planck-Institut für Biochemie, Am Klopferspitz 18a, 82152 Martinsried, Germany

Received August 27, 1996; Revised Manuscript Received December 4, 1996[⊗]

ABSTRACT: Conformational stability of the membrane-binding protein annexin V E17G has been determined by high-sensitivity differential scanning microcalorimetry (DSC) measurements and by isothermal, guanidinium hydrochloride (GdnHCl)-induced unfolding studies. Wild-type annexin V and the E17G mutant protein studied here are structurally almost identical. Therefore, it can be expected that the present results will not deviate significantly from the stability data of the wild-type molecule. Thermal unfolding is irreversible, while GdnHCl unfolding shows a high degree of reversibility. We were able to demonstrate that characteristic features of annexin V E17G unfolding permit us to extract from the kinetically controlled heat capacity curves thermodynamic equilibrium parameters at the high heating rates. The thermodynamic quantities obtained from the DSC studies in phosphate buffer at pH 7.0 are as follows: $t_{1/2} = 54.7$ °C (heating rate of 2.34 K min^{-1}), $\Delta H° = 690$ kJ mol^{-1}, and $\Delta C_p = 10.3$ kJ mol^{-1} K^{-1} which correspondends to a value of $\Delta G°_D$ (20 °C) of 53.4 kJ mol^{-1}. When compared on a per gram basis, these thermodynamic parameters classify annexin V E17G as a marginally stable protein. This conclusion is consistent with structural and functional features of the protein that require conformational adaptability for hinge-bending motions and pore formation on interaction with membranes. We observed a large difference between the change in the Gibbs energy value derived from the heat capacity studies and that determined from the GdnHCl unfolding curve. The difference appears to stem from a specific interaction of the protein with the denaturant that results in both a low half-denaturation concentration $c_{1/2}$ of 1.74 M and a small slope (6.0 kJ L mol^{-2}) of the ΔG_{app} versus [GdnHCl] plot. The extraordinary interaction of annexin V with GdnHCl is also manifested in the enormous depression of the transition temperature $\Delta t_{1/2}$ (=18 °C) when the GdnHCl concentration is increased from 0 to 1 M. "Regular" proteins experience an average decrease in the transition temperature of 8 ± 2 °C per 1 M change in the concentration of GdnHCl.

The annexins comprise a group of cytosolic, "bivalent" proteins of high structural homology that bind to negatively charged membranes in the presence of Ca^{2+} ions. The various annexins differ only by their N-terminal sequence which is responsible for the differences in their function (Creutz, 1992). Annexins exhibit anticoagulatory and antiinflammatory activities, and they are supposedly involved in membrane fusion and exocytosis as well as in the interaction between the cytoskeleton and the membrane. Annexin V and VII are Ca^{2+}-dependent membrane-binding proteins that can form voltage-dependent Ca^{2+} channels in phospholipid bilayers (Pollard & Rojas, 1988; Karshikov et al., 1992; Berendes et al., 1993; Demange et al., 1994). Annexin III catalyzes hydrolysis of the 1,2-cyclic inositol phosphates (Ross et al., 1990; Creutz, 1992).

Binding studies of annexin V with model membranes have shown that the association step is followed by trimer formation and a higher degree polymerization and finally leads to quasi-crystalline two-dimensional domains on the membrane surface. In these domains, six trimers form hexameric structures similar to a triscelion motif (Mosser et al., 1991; Brisson et al., 1991; Concha et al., 1992; Voges et al., 1994; Pigeault et al., 1994).

The crystal structure of annexin V (PAP, Funakoshi et al., 1987; PP4, Grundmann et al., 1988) has been solved by Huber and collaborators (Huber et al., 1990a,b, 1992). Annexin V from human placenta contains 320 amino acids with a molar weight of 35 730. Three hundred sixteen amino acids are visible in the X-ray picture (1AVR, Brookhaven Protein Data Bank). The structure of human annexin V is shown in Figure 1. In the upper part, the structure is viewed parallel to the membrane which would be located at the convex side that contains the calcium binding sites shown as pink spheres. The protein is largely α-helical, contains no carbohydrates, and has no disulfide bridges. It consists of four repeats of approximately 70 amino acids (lower part of Figure 1) which form a planar-cyclic arrangement. The four repeats are arranged in two structurally distinguishable modules consisting of the repeats I (blue), IV (cyan), and II (red), III (green), respectively, which can perform hinge-like movements with respect to each other (Huber et al., 1992). The repeats are highly homologous, and each consists

[†] This work was supported by grants from the Deutsche Forschungsgemeinschaft (to H.-J.H., Hi 204/22.1).

[‡] Coordinates have been deposited in the Brookhaven Protein Data Bank under file name 1AVR.

* Corresponding author. Phone: (49) 251/8323427. Fax: (49) 251/8329163. E-mail: hinz@nwz.uni-muenster.de.

[⊗] Abstract published in *Advance ACS Abstracts,* February 1, 1997.

S0006-2960(96)02163-0 CCC: $14.00

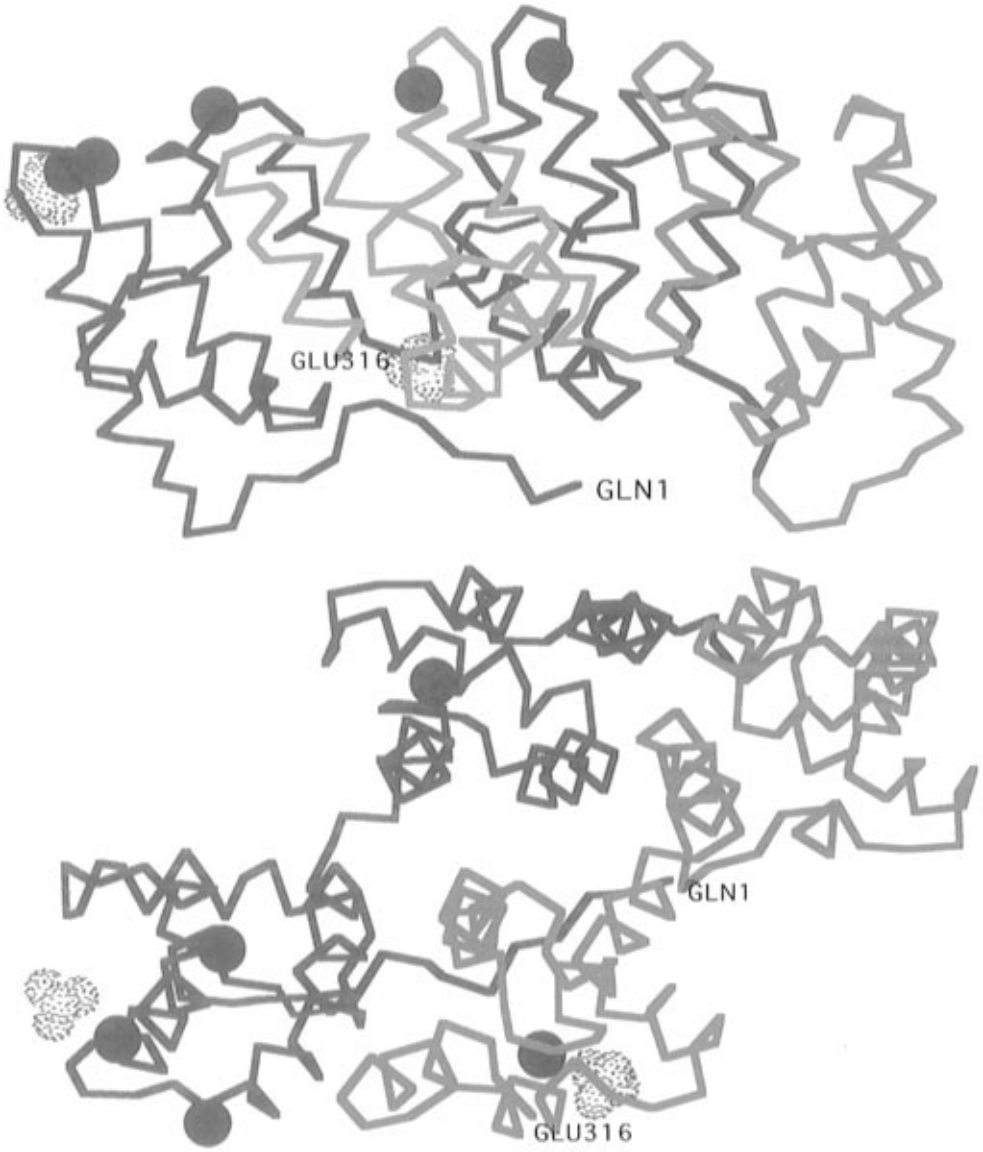

FIGURE 1: (top) Backbone structure of annexin V from human placenta (1AVR, Brookhaven Data Bank; Huber et al., 1992). The four domains are labeled with different colors: repeat I, blue; repeat II, red; repeat III, green; and repeat IV, cyan. The Ca^{2+} binding sites are marked as pink spheres. They occur at the convex side of the molecule. The dotted spheres refer to sulfate binding sites. The sixth Ca^{2+} binding site becomes only available after saturation of the others. For better orientation, the first and the last amino acid are labeled. (bottom) View from the membrane site at the annexin V molecule. The four-helix bundle structure of the repeats is particularly well illustrated in domain II (red).

of five α-helical segments with two to four helical coils which are wound into a right-handed, rather compact superhelix.

Repeats I, II, and IV contain three high-affinity Ca^{2+} binding sites at protruding loops similar to those in phospholipase A_2 and two Ca^{2+} binding sites of lower affinity that become available at higher Ca^{2+} concentrations (Huber et al., 1992). The sulfate binding sites present in the crystal may not be of great relevance under physiological conditions. Interaction of annexin V with the membrane is assumed to occur via binding of the convex metal site containing part of the molecule to negatively charged phospholipids (Voges et al., 1994; Andree et al., 1992, 1993; Bazzi & Nelsestuen, 1992; Blackwood & Ernst, 1990; Junker & Creutz, 1993; Gilmanshin et al., 1994). This reaction is associated with an injection of tryptophan 187 into the double layer. The movement of the tryptophan is manifested by strong quenching of tryptophan fluorescence at around 350 nm, which has been used extensively as a conformational probe in solution studies (Meers, 1990; Meers & Mealy, 1993a,b, 1994). The synergistic effects of local electric fields and the assumed perturbation of the phospholipid bilayer by the tryptophan are visualized as the causative reactions of ion channel formation. Both binding of Ca^{2+} to annexin V and the interaction of the protein with the surface of the membrane are associated with further structural changes of the protein (Gerstein et al., 1994). In addition to the movement of W187 by 18 Å, high Ca^{2+} concentrations apparently lead to rearrangements of Ca^{2+} binding sites and modulation of affinity constants (Sopkova et al., 1993, 1994; Burger et al., 1994; Lewitt-Bentley et al., 1992, 1994). The asymmetric distribution of calcium binding sites is shown in Figure 1 (Concha et al., 1993). In the absence of phospholipid vesicles, high Ca^{2+} concentrations lead to dimer formation of annexin V (Neumann et al., 1994; Ahn et al., 1988).

Recent X-ray and mutational studies by Huber and collaborators (Burger et al., 1994) provided detailed insight into the structural basis of the ion channel. The central pore is characterized by the occurrence of a four-helix-bundle

structure (domain II and IV) that contains at the inside 12 conserved charged or hydrophilic residues [His267, Glu95 (selectivity filter), Arg271, Glu112 (voltage gate), Asp92, and Arg117] as well as highly conserved, ordered water molecules. The electrophysiological analysis of the *in vitro* ion selectivity and voltage-gating properties of annexin V in the presence of model membranes fully supports the structural interpretation of the pore function.

The detailed functional and structural molecular picture contrasts with the relatively poor information on the energetic basis of the various conformational changes instrumental in Ca^{2+} binding and interaction with the membrane. In the present study, we set out to characterize the stability of annexin V in the absence of Ca^{2+} ions as the basis for further studies on functionally and structurally significant mutants and on the interaction of these proteins with Ca^{2+} ions and membranes. We determined the thermally induced denaturation of annexin V by DSC[1] measurements and followed the GdnHCl-promoted un- and refolding by CD studies. Despite the irreversibility of the thermal unfolding reaction, we have demonstrated that for this system the kinetically controlled heat capacity functions can be used for the extraction of equilibrium parameters which permit calculation of the stability of annexin as a function of temperature.

MATERIALS AND METHODS

Protein. We employed mainly the E17G mutant of annexin V expressed in *Escherichia coli* in our studies, because this mutant is structurally indistinguishable from the wild-type protein and can be produced in large quantities with relative ease (Burger et al., 1994). The concentration of the protein was determined by using an absorption coefficient ϵ of 0.60 cm^2 mg^{-1} (Gill & van Hippel, 1989; Perkins, 1986). Molar quantities have been calculated employing a molar mass of 35 730 g mol^{-1}. The following buffers were used in the measurements: (a) 20 mM sodium phosphate at pH 3.0−8.0 and (b) 50 mM Tris and 100 mM potassium chloride at pH 8.0 (at 20 or 25 °C). Prior to all measurements, samples were dialyzed to equilibrium in a buffer containing EGTA followed by dialysis against the corresponding buffer.

Chemicals. All chemicals used were of reagent grade quality. GdnHCl, ultra pure, was purchased from Schwarz/Mann (Cleveland, OH). Quartz-bidistilled water was used throughout this work.

DSC Studies. Differential scanning heat capacity studies have been performed with electronically modified Privalov-type DASM4 microcalorimeters (Privalov et al., 1980) in the temperature range from 5 to 110 °C. Due to the irreversibility of the transitions, the heat capacity peaks exhibit a variation in the shape and transition temperature with heating rate. For the analysis of these kinetic effects, we used different heating scan rates (0.125, 0.589, 1.004, 1.189, 1.99, and 2.345 K min^{-1}).

Heat capacity and temperature data pairs were routinely taken every 0.1 K using a Keithley DMM192 voltmeter and were stored on a personal computer. The specific C_p value was calculated using a value of 0.74 mL g^{-1} for the partial specific volume of the sample.

Typical protein concentrations for the calorimetric experiments were between 0.5 and 1.2 mg mL^{-1} (1.40−3.359 μM). Each sample run was preceded by a baseline run with buffer-filled cells. Electrical calibration of the instrument was performed using 50 μW power signals. Integration of the transition curves was done numerically. Molar transition enthalpies, ΔH_{cal}, refer to M = 35 730 g mol^{-1}, and the van't Hoff enthalpies, ΔH_{vH}, have been calculated according to the van't Hoff equation for a monomolecular process

$$\Delta H_{vH}(T_{1/2}) = 4RT_{1/2}^2 \frac{C_p(T_{1/2})}{\Delta H_{cal}(T_{1/2})} \quad (1)$$

where $T_{1/2}$ represents the midpoint temperature (at 50% of the peak area) of the unfolding reaction, $C_p(T_{1/2})$ and $\Delta H_{cal}(T_{1/2})$ are, respectively, the molar excess heat capacity and transition enthalpy at $T_{1/2}$, and R is the gas constant (R = 8.3144 J mol^{-1} K^{-1}). It should be mentioned here that, due to the dependence of $\Delta H_{vH}(T_{1/2})$ on the shape of the transition curves, numerical values obtained from transition curves measured at low heating rates (<1 K min^{-1}) are meaningless and have not been included in the tables.

CD Measurements. CD studies were carried out with a CD6 Jobin Yvon spectropolarimeter. Unless otherwise stated, spectra were averaged over four scans and corrected for the buffer signal. A CD cuvette with an optical path length of 1 cm was used to monitor the GdnHCl-induced unfolding at a wavelength of 222 nm. For all measurements, buffers were degassed and the sample compartment was thoroughly purged with a constant flow of nitrogen (5 L min^{-1}). The instrument was calibrated with d(+)-camphorsulfonic acid that had been twice recrystallized from glacial acetic acid. A value of 188 mdeg was used for the ellipticity at 290 nm, employing a 0.6 mg mL^{-1} solution in a 1 cm cuvette (Yang et al., 1986; Schmid, 1989). The temperature was controlled and monitored using a 100 Ω platinum resistance thermometer immersed in the protein solution.

RESULTS

Wild-Type Annexin V and the E17G Mutant Show Identical C_p Transition Curves

The exchange of glutamate 17 by glycine was supposed to involve negligible structural and energetic perturbation, since position 17 occurs at the surface of the protein (Burger et al., 1994). This expectation is verified by the comparison of heat capacity scans of the wild-type and mutant protein shown in Figure 2. The thermodynamic parameters are summarized in Table 1. Transition temperatures and calorimetric and van't Hoff enthalpy values are very similar for the wild-type and mutated protein. This is supportive evidence for the negligible perturbation associated with this amino acid exchange.

[1] Abbreviations: annexin V E17G, mutant of annexin V with amino acid replacement of Glu17 by Gly; annexin V-wt, wild-type annexin V; DSC, differential scanning calorimetry; CD, circular dichroism; C_p, apparent molar heat capacity; ΔC_p, heat capacity change on unfolding; $\Delta_t C_p$, transitional molar heat capacity; ΔH_{cal}, calorimetric enthalpy of unfolding; ΔH_{vH}, van't Hoff enthalpy of unfolding; $t_{1/2}$ (in degrees Celsius), temperature of 50% conversion; $\Delta H°$, molar standard change in enthalpy of unfolding; $\Delta G°_D$, molar standard change in Gibbs energy of unfolding; $T_{1/2}$ (in kelvin) = $t_{1/2}$ + 273.15 and T^* (in kelvin) = t^* + 273.15.

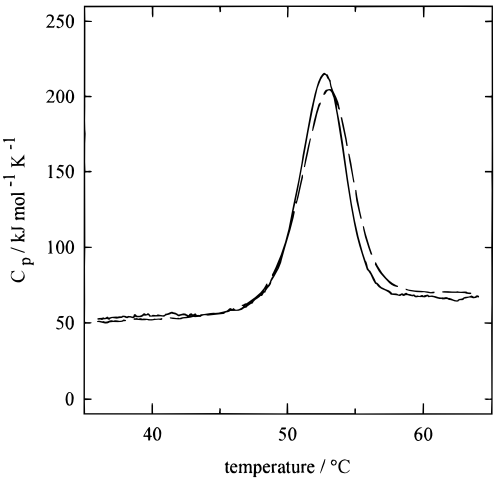

FIGURE 2: Irreversible C_p transition curves of annexin V [wild type (—) and mutant E17G (− − −)]. The buffer was 50 mM Trisand 100 mM KCl at pH 8.0 (25 °C); protein concentrations were as follows: wild type, $c = 0.42$ mg mL^{-1}; and mutant, $c = 0.99$ mg mL^{-1}. The heating was rate 1.99 K min^{-1}.

Table 1: Comparison of Thermodynamic Transition Parameters of the Wild Type and the E17G Mutant Protein of Annexin V[a]

annexin V	$t_{1/2}$ (°C)	ΔH_{cal} (kJ mol^{-1})	ΔH_{vH} (kJ mol^{-1})
wild type	52.5 ± 0.5	682 ± 18	794 ± 25
E17G	52.8 ± 0.5	686 ± 25	725 ± 15

[a] The data refer to the C_p transition curves shown in Figure 2. The heating rate was 1.99 K min^{-1}. The buffer was 50 mM Tris and 100 mM KCl at pH 8.0 (25 °C).

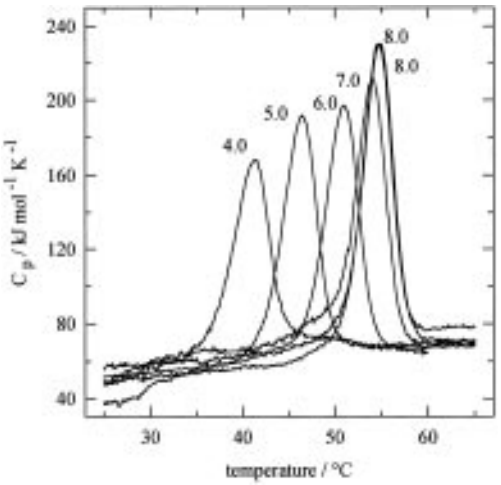

FIGURE 3: Irreversible C_p transition curves of annexin V E17G as a function of pH (4−8). Protein concentrations between 0.41 and 1.23 mg mL^{-1} were used; the heating rate was 1.19 K min^{-1}. The reproducibility of independent measurements under identical conditions is demonstrated by the coincidence of the C_p curves at pH 8.0. The buffer was 20 mM sodium phosphate.

Transition Curves of Annexin V E17G Are Shifted toward Higher Temperatures with Increasing pH

Figure 3 shows DSC scans as a function of the pH of the solution. The transition of annexin V (E17G) occurs at 40.6 °C at pH 4.0 and shifts to 54.4 °C at pH 8.0. The thermodynamic parameters of the transitions are summarized in Table 2. All curves are decidedly irreversible as indicated by the absence of any heat capacity peak in the second heating of a sample solution (scans not shown). There is, however, a distinctive feature of the curves that renders them

Table 2: Variation of Thermodynamic Transition Parameters of Annexin V E17G with pH[a]

pH	$t_{1/2}$ (°C)	ΔH_{cal} (kJ mol^{-1})	ΔH_{vH} (kJ mol^{-1})	$\Delta H_{cal}/\Delta H_{vH}$
8.0	54.4 ± 0.5	679 ± 31	831 ± 35	0.82
7.2 (52.0 °C)*	52.0 ± 0.5	674 ± 25	777 ± 15	0.87
7.0	53.4 ± 0.5	680 ± 9	791 ± 1	0.86
6.0	50.5 ± 0.5	616 ± 2	726 ± 4	0.85
5.0	46.1 ± 0.4	619 ± 10	712 ± 8	0.87
4.0	40.6 ± 0.1	537 ± 18	633 ± 4	0.85

[a] The buffer was 20 mM sodium phosphate. The * indicates a measurement using Tris buffer, which had a starting pH of 8.0 at 25 °C. At 52 °C, this corresponds to a pH value of 7.2. The heating rate was 1.19 K min^{-1}. At each pH value, two to four measurements were performed.

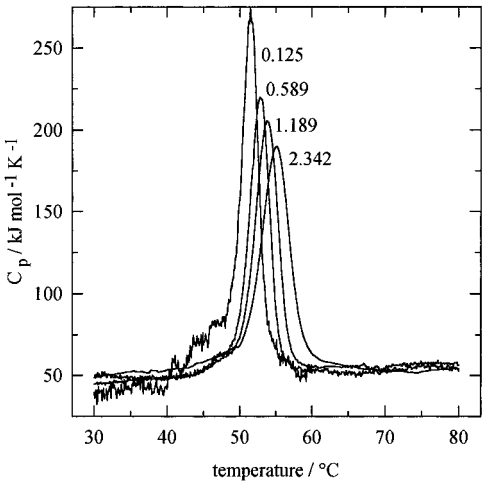

FIGURE 4: Variation with heating rate of the C_p transition curves of annexin V E17G. The numbers near the peaks refer to the heating rates in kelvin per minute. The buffer was 20 mM sodium phosphate at pH 7.0. The protein concentrations of the respective measurements were as follows: 0.125 K min^{-1}, $c = 0.49$ mg mL^{-1}; 0.589 K min^{-1}, $c = 0.67$ mg mL^{-1}; 1.189 K min^{-1}, $c = 0.67$ mg mL^{-1}; and 2.342 K min^{-1}, $c = 0.67$ mg mL^{-1}.

particularly suitable for theoretical analysis. Irreversibility is not associated with exothermic phenomena as is frequently observed with aggregating systems. In such cases, the high-temperature part of the heat capacity peak is usually asymmetric and drops precipitously below the heat capacity function of the unfolded state, before gradually leveling off at the unfolded state heat capacity of the aggregated system. It is evident that the shape of the C_p transition curves of annexinV E17G exhibits no such characteristics of irreversibility. All transition curves show remarkably high cooperativity as demonstrated by the small transition range of 10−12 °C and are characterized by a small apparent ΔC_p of only about 10 kJ mol^{-1} K^{-1}. The reproducibility of independent measurements under identical conditions is excellent as demonstrated by the two curves at pH 8.0 in Figure 3.

Despite the Irreversibility of the Transition Equilibrium Thermodynamic Parameters Can Be Derived from the Annexin Transition

The kinetic control of annexin V E17G unfolding is illustrated in Figure 4 which shows C_p transition curves as a function of heating rate (rates given at each transition curve). The maximum of the C_p curve is shifted toward lower temperatures with a decrease in the scan rate.

Table 3: Variation of Apparent Thermodynamic Transition Parameters of Annexin V E17G with Heating Rate[a]

heating rate (K min^{-1})	$t_{1/2}$ (°C)	ΔH_{cal} (kJ mol^{-1})	ΔH_{vH} (kJ mol^{-1})	$\Delta H_{cal}/\Delta H_{vH}$
0.125	51.1	695	993	0.70
0.589	52.5	671	872	0.77
1.189	53.4	671	792	0.85
2.342	54.7	690	683	1.01

[a] The buffer was 20 mM sodium phosphate at pH 7.0.

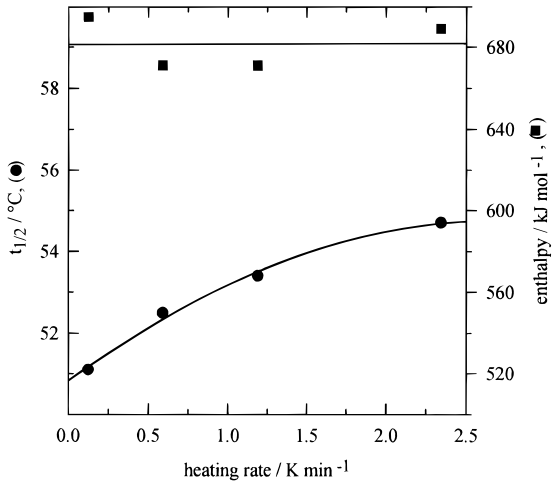

FIGURE 5: $t_{1/2}$ values (left ordinate, ●) and transition enthalpies (right ordinate, ■) of annexin V E17G as a function of heating rate in 20 mM sodium phosphate buffer at pH 7.0. Heating rates (kelvin per minute) and protein concentrations (milligrams per milliliter) were the same as in Figure 4. Enthalpy data have been fitted to a polynomial of the first degree and $t_{1/2}$ values to one of the second degree.

Concomitantly, the transition peak becomes less symmetric and the half-width decreases. However, notably, the post-transitional baseline does not change which suggests that the aggregation phenomena which start within the transition range proceed with no detectable thermal effects. Standard numerical integration of the transition curves and determination of $t_{1/2}$ at 50% conversion yields the parameters presented in Table 3. The graphical representation of the data is provided in Figure 5, where both the calorimetric transition enthalpies and transition temperatures obtained at different heating rates are plotted versus scan rate. One recognizes a pronounced dependence of the $t_{1/2}$ values on scan rate (filled dots), whereas the concomitant transition enthalpies are within error limits independent of scan rate (filled squares). The negligible influence of scan rate on the transition enthalpy is also numerically evident if one implies a linear dependence according to eq 2

$$\Delta H_{cal} = a + br \tag{2}$$

Linear least-squares calculations yield the following values for the parameters: $a = 681$ kJ mol^{-1} and $b = 0.212$ kJ min mol^{-1} K^{-1}. The small value of b permits one to neglect this correction to a first approximation and consider ΔH_{cal} practically scan rate-independent. This does not apply to the $t_{1/2}$ temperature values, as the plot of transition temperature versus scan rate shown in Figure 5 illustrates. The transition temperatures have been fitted to a second-order polynomial in scan rate r

$$t_{1/2} = c + dr + er^2 \tag{3}$$

with the following values of the coefficients: $c = 50.82$ °C, $d = 2.891$ min, and $e = -0.530\,25$ min^2 K^{-1}. Inspection of the function shows that at a heating rate of 2.342 K min^{-1} the transition temperature has practically reached its maximum value and that further increases in the heating rate do not change this value significantly. Furthermore, the van't Hoff enthalpy approaches the true calorimetric enthalpy with the increasing heating rate, thereby rendering the cooperativity ratio $\Delta H_{cal}/\Delta H_{vH}$ equal to 1.

It is of fundamental significance to ask the following question. Can equilibrium parameters be deduced from the transition, in view of the irreversibility of the unfolding process? Irreversible steps are kinetically controlled and are therefore not accessible to treatment by equilibrium thermodynamics. However, assuming a model for the irreversible process and the rate-limiting step that allows one to delineate the conditions under which standard equilibrium thermodynamic analysis of the heat capacity functions is justified and often permissible.

The simplest model conceivable, which nevertheless is frequently in accordance with experimental observations, was first employed by Lumry and Eyring (1954). It assumes reversible unfolding of the protein followed by a rate-limiting irreversible step as shown in eq 4.

$$\mathrm{N} \underset{k_{-1}}{\overset{k_1}{\rightleftharpoons}} \mathrm{D} \xrightarrow{k_2} \mathrm{I} \tag{4}$$

The extent of irreversibility at a given temperature and time is determined by the rate of the D → I step. This model forms the basis of the elaborate treatments of irreversible DSC measurements by Sanchez-Ruiz and collaborators (Sanchez-Ruiz et al., 1988; Freire et al., 1990; Guzmán-Casado et al., 1990; Conejero-Lara et al., 1991a,b; Galisteo et al., 1991; Sanchez-Ruiz, 1992; Galisteo & Sanchez-Ruiz, 1993).

We employed their equations to demonstrate that for annexin V E17G, at the high heating rate, conditions are such that the thermodynamic parameters obtained from the standard treatment of the heat capacity curves (integration of area, van't Hoff calculation according to eq 1, $t_{1/2}$ determination at 50% of the area under the peak) are a valid representation of the energetics of equilibrium unfolding of annexin V (E17G).

The pattern of scan rate dependence of DSC curves observed here for annexin unfolding is very similar to that given in Figure 4 of the article by Sanchez-Ruiz (1992). The author also assumes the validity of the Lumry−Eyring model for the irreversible process, i.e. a first-order irreversible reaction as the rate-limiting step after a reversible unfolding equilibrium. The temperature dependence of the first-order rate constant k_2 is given by the Arrhenius equation

$$k_2 = \exp\left[-\frac{E_A}{R}\left(\frac{1}{T} - \frac{1}{T^*}\right)\right] \tag{5}$$

where E_A is the activation energy, T^* is the temperature at which the rate constant is unity [$k_2(T^*) = 1$ s^{-1}], R is the gas constant, and T is the experimental temperature in kelvin.

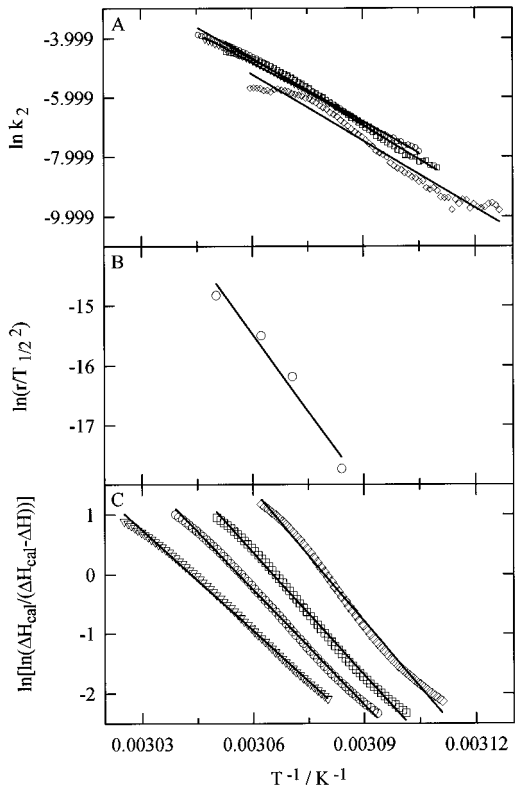

FIGURE 6: Determination of activation parameters from the experimental heat capacity functions. Methods according to Sanchez-Ruiz et al. (1988).

Determination of Activation Parameters

In the Lumry−Eyring scheme (eq 4), one assumes $k_2 < k_{-1}$ as well as $k_2 < k_1$. Then k_2 is the rate-limiting step, and its activation energy can be considered to determine the variation with temperature of the rate of unfolding. Four different methods have been devised by Sanchez-Ruiz et al. (1988) for a proper evaluation of the activation energy from heat capacity curves. We applied all of them, because each has definite advantages and disadvantages. The graphical representations of evaluations according to methods A−C are shown in Figure 6A−C.

Method A. The rate constant k_2 (inverse seconds) is obtained at each temperature from the following equation

$$k_2 = \frac{rC_p}{\Delta H_{cal} - \Delta H} \tag{6}$$

where r refers to the heating rate in kelvin per second, C_p is the molar heat capacity, ΔH (kilojoules per mole) is the corresponding enthalpy at T, and ΔH_{cal} is the total molar transition enthalpy. The activation energy is obtained from the Arrhenius equation

$$k_2 = A \exp\left(-\frac{E_A}{RT}\right) \tag{7}$$

where $A = \exp(E_A/RT^*)$, the frequency factor in inverse seconds. For each heating rate, k_2 was evaluated for all data in the interval $(T_{1/2} - 3) \leq T \leq (T_{1/2} + 3)$. The Arrhenius plots are shown in Figure 6A. The mean and standard deviation of the activation energy of annexin V E17G obtained from the slopes of the Arrhenius plots are as follows

$$E_A(A) = 601 \pm 35 \text{ kJ mol}^{-1}$$

Method B. The variation of the transition temperature, $T_{1/2}$, with heating rate is given by the following relationship

$$\frac{r}{(T_{1/2})^2} = \frac{AR}{E_A} \exp\left(-\frac{E_A}{RT_{1/2}}\right) \tag{8}$$

A plot of $\ln[r/(T_{1/2})^2]$ versus $1/T_{1/2}$ should yield a straight line with a slope of $-E_A/R$. The activation energy obtained from the slope of the plot shown in Figure 6B is as follows

$$E_A(B) = 713 \pm 95 \text{ kJ mol}^{-1}$$

Method C. The third estimate of E_A stems from the following relationship. It has been shown (Sanchez-Ruiz et al., 1988) that eq 9 holds:

$$\ln\left[\ln\left(\frac{\Delta H_{cal}}{\Delta H_{cal} - \Delta H}\right)\right] = \frac{E_A}{R}\left(\frac{1}{T_{1/2}} - \frac{1}{T}\right) \tag{9}$$

Plotting the left side of eq 9 versus $1/T$ should yield a straight line with a slope of $-E_A/R$ for each heating rate. The results are shown in Figure 6C. The average value of the activation energy obtained from the four slopes is as follows

$$E_A(C) = 546 \pm 50 \text{ kJ mol}^{-1}$$

Method D. Finally, the activation energy can be evaluated from the heat capacity at the transition temperature, $C_p(T_{1/2})$, using the equation

$$E_A(D) = \frac{eRC_p(T_{1/2}){T_{1/2}}^2}{\Delta H_{cal}} \tag{10}$$

The value obtained is as follows

$$E_A(D) = 586 \pm 120 \text{ kJ mol}^{-1}$$

The value of the activation energy averaged over the results obtained from the four methods is as follows

$$\bar{E}_A = 611 \pm 70 \text{ kJ mol}^{-1}$$

It is obvious that the error involved in the determination of the activation energy is relatively large. It can be reduced, if the value of E_A that was obtained with the lowest heating rate in method B is not considered in the averaging procedure. Then one would obtain a value of 567 ± 30 kJ mol^{-1}. However, irrespective of which of the two average values is chosen, the most significant result of these evaluations is that the activation energy is among the largest observed so far for proteins. In the few quantitative studies published to date, activation parameters of protein unfolding range between 280 and 360 kJ mol^{-1}, and therefore, E_A was found to be practically independent of the nature of the individual protein (Sanchez-Ruiz et al., 1988; Guzmán-Casado et al., 1990; Conejero-Lara et al., 1991a,b; Galisteo et al., 1991; Sanchez-Ruiz, 1992; Galisteo & Sanchez-Ruiz, 1993). Bacteriorhodopsin at pH 7.5 is an exception with an activation energy of 731 ± 36 kJ mol^{-1}, which is twice that of the transition enthalpy of 346 ± 22 kJ mol^{-1}. At pH 9.5,

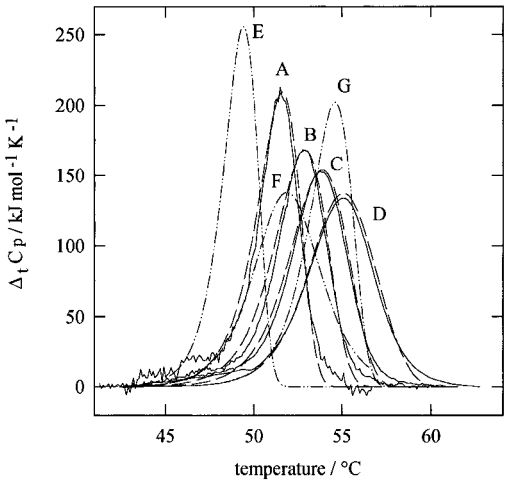

FIGURE 7: Comparison of experimental (solid lines) and simulated transition curves (dashed and dotted dashed lines). The simulated curves have been calculated using eqs 5, 11, and 12 with the parameters summarized in Table 4.

the activation energy drops to 361 ± 15 kJ mol^{-1} (Galisteo & Sanchez-Ruiz, 1993).

The large activation barrier for annexin V E17G unfolding implies that the protein must unfold to a large extent before irreversible, athermal aggregation sets in. It is possible to calculate the transitional molar heat capacity, $\Delta_t C_p$, numerically on the basis of the Lumry−Eyring model using the following equation (Sanchez-Ruiz, 1992)

$$\Delta_t C_p = \frac{K\Delta H^\circ}{(K+1)^2}\left(\frac{k_2}{r} + \frac{\Delta H^\circ}{RT^2}\right)\exp\left(-\frac{1}{r}\int_{T_o}^{T}\frac{k_2 K}{K+1}\mathrm{d}T\right) \quad (11)$$

$$K = \frac{[\mathrm{D}]}{[\mathrm{N}]} = \exp\left[-\frac{\Delta H^\circ}{R}\left(\frac{1}{T} - \frac{1}{T_{1/2}}\right)\right] \quad (12)$$

where $\Delta_t C_p$ is the transitional molar heat capacity, K is the equilibrium constant of the reversible unfolding reaction, k_2 (inverse seconds) is the first-order rate constant defined by eq 7, ΔH° is the standard transition enthalpy which, for annexin V E17G, is practically identical to the ΔH_{cal} value, r is the heating rate in kelvin per second, and T_o is the temperature at which no detectable heat absorption occurs. The reversible part of the transitional heat capacity is given by the equation

$$\Delta_t C_{p,\mathrm{rev}} = \frac{(\Delta H^\circ)^2}{RT^2}\frac{K}{(K+1)^2} \quad (13)$$

The residual part of eq 11 describes the influence of the irreversible process. For application of eq 11, one requires numerical values of k_2, K, ΔH°, $T_{1/2}$, E_A, and T^*, all of which can be calculated from the heat capacity scans. T^* can be obtained using eq 7 (method A) which provides an axial section of E_A/RT^*. For all four heating rates, we obtained identical activation energies and very similar T^* values of 335.1 ± 1.1 K, which corresponds to 61.9 ± 1.1 °C. This result shows that T^*, depending on the heating rate, lies by 7.2−10.8 °C above the apparent transition temperature $T_{1/2}$ which means that the transition is practically finished before the denaturation rate constant reaches a value of unity.

Figure 7 shows the results of some curve simulations based on eq 11 using the parameters summarized in Table 4.

Table 4: Thermodynamic and Kinetic Parameters Employed in the Simulation of the Heat Capacity Transition Curves Shown in Figure 7[a]

curves in Figure 7	heating rate (K s^{-1}) (K min^{-1})	ΔH_{cal} (=ΔH°) (kJ mol^{-1})	$t_{1/2}$ (°C)	E_A (kJ mol^{-1})	t^* (°C)
A	2.0833×10^{-3} (0.125)	695	51.9	601	60.9
B	9.9667×10^{-3} (0.589)	671	52.9	601	60.9
C	19.817×10^{-3} (1.189)	671	53.8	601	61.5
D	39.033×10^{-3} (2.342)	690	54.7	601	63.0
E	2.0833×10^{-3} (0.125)	695	51.9	300	60.9
F	1 (60)	695	51.9	601	60.9
G	39.033×10^{-3} (2.342)	690	54.7	601	59.0

[a] Equations 5, 11, and 12 were used for the calculation of the temperature dependence of the transitional heat capacity, $\Delta_t C_p$.

Equation 11 has been derived for a temperature-independent transition enthalpy. Therefore, a coordinate transformation was applied to the C_p functions to remove the ΔC_p under conservation of the area under the transition peak. These transformed transition curves are shown in Figure 7 with solid lines, while the simulated curves are shown with dashed lines. Inspection of Figure 7 shows that there is good agreement between experimental and theoretical transition curves. Such good agreement requires careful variation of the parameters in eq 11, because the value of $\Delta_t C_p$ is highly sensitive to small changes in these quantities. Formally, one can always obtain apparently perfect fits by application of iteration procedures which permit free variation of all parameters. The resulting quantities do not, however, necessarily reflect the thermodynamic reality correctly. The sensitivity to small changes in the parameters is illustrated by the fact that we had to use the temperatures of the maximum of the heat capacity peaks, not the $T_{1/2}$ values at 50% of the peak area, in order to optimize the calculations. Due to the asymmetry of the transition peaks, particularly at low heating rates, $T_{1/2}$ values are slightly smaller (up to 0.8 K) than the temperatures of the peak maximum. This difference is of significance in the peak calculation procedures using eq 11. In contrast, the choice of T_o is not critical, provided it is below the start of the transition.

As a general result, the asymmetry of the transition peaks can be influenced by a variation in the magnitude of the activation energy and also by a variation of the T^* value. Since the activation energy is determined from the slope of the Arrhenius plot (eq 5) and T^* is determined from the axial section, which is $k^* = E_A/RT^*$, it is obvious that these two parameters are not independent.

Peaks E−G in Figure 7 illustrate the effects on the heat capacity functions of changes in the activation energy, the heating rate, and the magnitude of T^*, respectively. If one decreases the activation energy from 601 kJ mol^{-1} to the frequently observed value of 300 kJ mol^{-1} with all other parameters kept identical, curve A is transformed into curve E. The maximum of the transition peak is increased and shifted considerably to lower-temperature and the shape is significantly more asymmetric at the high-temperature shoulder than that of the experimental curve. If, on the other hand, the heating rate is increased from 2.0833×10^{-3} to 1 K s^{-1} (60 K min^{-1}), while the other parameters remain constant, curve F is obtained. This transition curve is fully symmetric and identical in shape to transition curve D, which is the experimental curve measured with a heating rate of 2.342 K min^{-1}. This result illustrates the fact that a high

heating rate overcompensates for the effects of irreversibility in the C_p curves of annexin V E17G.

The influence of a decrease in T^* by 4 °C is demonstrated by curve G. Except for the lower T^* value, all other parameters are the same as used in calculation of curve D.

The results of these simulation studies allow us to draw a very important conclusion. Extraction of transition enthalpies and transition temperatures from the heat capacity curves of annexin V E17G that were determined at heating rates of 1.189 and 2.342 K min^{-1} is obviously permissible, and considering these parameters to be identical to equilibrium quantities is also permissible. These quantities will be discussed in the subsequent section.

Stability Parameters of Annexin V E17G

The thermodynamic transition parameters obtained from analyses of the C_p curves measured at a scan rate of 1.19 K min^{-1} are summarized in Table 2. Evaluation of the van't Hoff enthalpy was based on a two-state process, since there is no visible evidence in the C_p curves for intermediate transitions, nor is it possible to perform a deconvolution of the experimental transition curves shown in Figure 3 into more than one transition. The small shoulder at the low-temperature side of the C_p curves cannot be treated separately and was therefore included in the overall peak integration to obtain the transition enthalpy. Comparison of the calorimetric and van't Hoff enthalpies shows that the van't Hoff enthalpies as deduced from eq 1 are consistently between 90−150 kJ mol^{-1} larger than the calorimetric values, which leads to a cooperativity ratio $\Delta H_{cal}/\Delta H_{vH}$ of 0.86 ± 0.03. The value is smaller than 1, and we assign this deviation from 1.0, in light of the previous discussion, to the consequences of the irreversibility of the transition rather than to any domain unfolding. It appears that at 1.19 K min^{-1} the shape of the transition curve is still slightly deformed in the sense that it is sharper than the equivalent equilibrium transition. Deviations from two-state unfolding as a consequence of independent subdomain unfolding would lead to broadening rather than sharpening of the transition and would therefore result in a ratio $\Delta H_{cal}/\Delta H_{vH}$ of >1.

The apparent specific transition enthalpy of 19.0 J g^{-1} at pH 7.0 and 8.0 is relatively small compared to values observed for other proteins. Together with the low transition temperature of about 53 °C at pH 7.0, this is suggestive of a relatively low intrinsic conformational stability of annexin V E17G.

The transition temperatures and enthalpies given in Table 2 permit us to determine the heat capacity change on unfolding from the slope of a plot of ΔH_{cal} versus transition temperature shown in Figure 8. The experimental transition enthalpies are precise to within ±5% and are illustrated by the closed circles. The straight line results from a linear least-squares treatment and gives an apparent molar heat capacity change ΔC_p of 10.3 ± 1.3 kJ mol^{-1} K^{-1} which corresponds to a ΔC_p per mole of residue (M_{res} = 320) of 32.2 J (mol of residue)$^{-1}$ K^{-1}. This value is relatively small when compared to per residue ΔC_p values of proteins of comparable size [α-amylase, ΔC_p = 76.2 J (mol of residue)$^{-1}$ K^{-1} (Oobatake & Ooi, 1993); pepsinogen, ΔC_p = 69 J (mol of residue)$^{-1}$ K^{-1} (Murphy et al., 1992); diphtheria toxin domain B, ΔC_p = 52.6 J (mol of residue)$^{-1}$ K^{-1} (Ramsey & Freire, 1990); subtilisin BPN′, ΔC_p = 73.0 J (mol of residue)$^{-1}$ K^{-1} (Pantoliane et al., 1989); and carbonic anhydrase, ΔC_p = 60.9 J (mol of residue)$^{-1}$ K^{-1} (Murphy et al., 1992)].

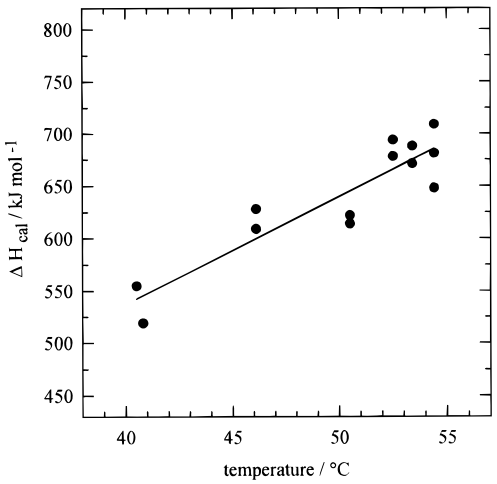

FIGURE 8: Variation with transition temperature, $t_{1/2}$, of the experimental transition enthalpy. The transition temperature has been shifted by varying the pH from 4.0 to 8.0. The closed circles refer to the experimental data ±5% error. The linear least-squares fit yields a ΔC_p of 10.3 ± 1.3 kJ mol^{-1} K^{-1}. The protein concentration was in the range of 0.41−1.23 mg mL^{-1}. The buffer was 20 mM sodium phosphate; the heating rate was 1.19 K min^{-1}.

Some small proteins show comparably low per residue ΔC_p values such as tendamistat (M = 7950 g mol^{-1}), ΔC_p = 39.2 J (mol of residue)$^{-1}$ K^{-1} (Renner et al., 1992); plasminogen fragment K4 (M = 9600), ΔC_p = 40.7 J (mol of residue)$^{-1}$ K^{-1} (Novokhatny et al., 1984); and ribonuclease T1 (M = 11 100), ΔC_p = 41.3 J (mol of residue)$^{-1}$ K^{-1} (Kiefhaber et al., 1990).

The only larger proteins which exhibit comparably small ΔC_p values are arabinose binding protein which has a ΔC_p = 43.8 J (mol of residue)$^{-1}$ K^{-1} (M = 34 300) (Oobatake & Ooi, 1993) and β-lactoglobulin which has a ΔC_p of 35 J (mol of residue)$^{-1}$ K^{-1} (M = 18 100) (Griko & Privalov, 1992). However, the value for β-lactoglobulin may need revision, since Ragone and Colonna (1994) reported recently a non-two-state transition for this protein.

Structurally, these small proteins are completely different from annexin, since their stability arises from a high degree of compactness and from the presence of disulfide bridges. In contrast, annexin V E17G has no covalent linkages and must be considered flexible rather than compact at least with regard to the hinge bending motions and the conformational mobility it demonstrates when it binds Ca^{2+} ions, attaches to membranes, and forms pores. Furthermore, the pores have been shown to contain a considerable number of conserved water molecules which might also counteract the formation of a hydrophobic core sequestered from solvent access. Since the latter would be a prerequisite for a large positive ΔC_p on unfolding, the small heat capacity change observed for annexin V E17G might actually be a direct consequence of the functional requirements of annexin V E17G which are conformational adaptability for Ca^{2+} and membrane binding associated with pore formation and large movements of a loop at the end of a helix (Gerstein et al., 1994). These structural and functional characteristics of annexin V provide also a plausible rationale for the occurrence of relatively small $t_{1/2}$ and $\Delta G°_D$ values.

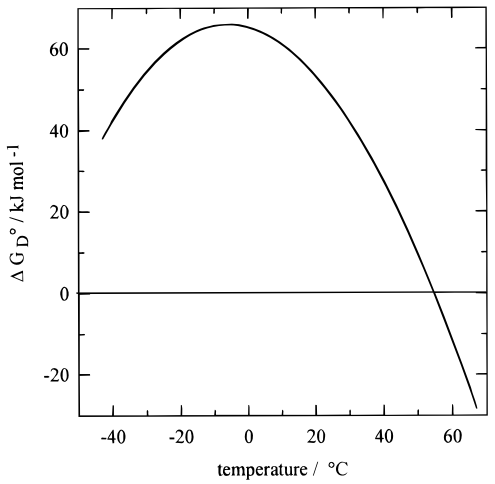

FIGURE 9: Gibbs energy of unfolding $\Delta G°_D$ of annexin V E17G as a function of temperature. The buffer was 20 mM sodium phosphate at pH 7.0. The stability curve has been calculated using eq 14 with the following parameters: $\Delta H_{cal} = 690$ kJ mol^{-1}, $\Delta C_p = 10.3$ kJ mol^{-1} K^{-1}, and $t_{1/2} = 54.7$ °C.

The stability curve, which represents the variation with temperature of the change in the standard Gibbs energy of unfolding, is shown in Figure 9. It was derived using eq 14 and the thermodynamic parameters at pH 7 given in Table 3 (heating rate of 2.34 K min^{-1}) and a ΔC_p of 10.3 kJ mol^{-1} K^{-1}.

$$\Delta G°_D(T) = \Delta H_{cal}(T_{1/2})\left(1 - \frac{T}{T_{1/2}}\right) - \Delta C_p T \ln \frac{T}{T_{1/2}} - \Delta C_p \times (T_{1/2} - T) \quad (14)$$

At 25 °C the $\Delta G°_D$ value of annexin V E17G is 48.3 kJ mol^{-1}, and at 20 °C, it is 53.4 kJ mol^{-1}. The stability maximum occurs around −5 °C and corresponds to 65.4 kJ mol^{-1}.

Isothermal Stability Studies on Annexin V E17G by GdnHCl Unfolding

It has been frequently observed that, in contrast to temperature-induced denaturation, chemical unfolding is a reversible process. Therefore, we performed GdnHCl-induced unfolding and refolding studies to probe the stability of annexin V against denaturants. Figure 10 shows unfolding and refolding curves of the protein at 20 °C monitored by ellipticity changes at 222 nm. The transition curves were analyzed using the linear extrapolation model for an N ↔ D isomerization reaction. The parameters obtained in the analysis are summarized in Table 5. The GdnHCl concentration corresponding to 50% unfolding, $c_{1/2}$, is about 1.74 M. This is a rather low value which is, however, consistent with the low transition temperature observed in the heat capacity studies.

The most unusual result of the isothermal denaturant unfolding studies is, however, the very low extrapolated change in the Gibbs energy value of $\Delta G°_D$ (buffer) of 10.4 ± 1.0 kJ mol^{-1} at 20 °C. This value is apparently incompatible with the value of about 53.4 kJ mol^{-1} derived from the DSC studies for thermal denaturation at the same temperature. One could argue that the ΔC_p value derived from the DSC studies might be erroneous, because heat release associated with the aggregation phenomena might have decreased the intrinsically larger denaturational heat capacity change, although, as discussed before, one does not observe the C_p characteristics usually involved in exothermic aggregation. But if, for the sake of the argument, we accept this hypothesis and assume that $\Delta G°_D$ (buffer) = 10.4 kJ mol^{-1}, calculated from the GdnHCl transition curve at 20 °C, is correct, we can calculate the ΔC_p value that would be compatible with this value and the thermal transition parameters, i.e. the transition temperature of 54.7 °C, where $\Delta G°_D$ is equal to 0, and the transition enthalpy of $\Delta H°$ (54.7 °C) = 690 kJ mol^{-1}. Since the transition enthalpy obtained from integration of the heat capacity peak does not vary with heating rate and since the transition temperature at the high heating rates becomes also independent of heating rate, both parameters, $\Delta H°$ and $T_{1/2}$, can be considered correct thermodynamic parameters.

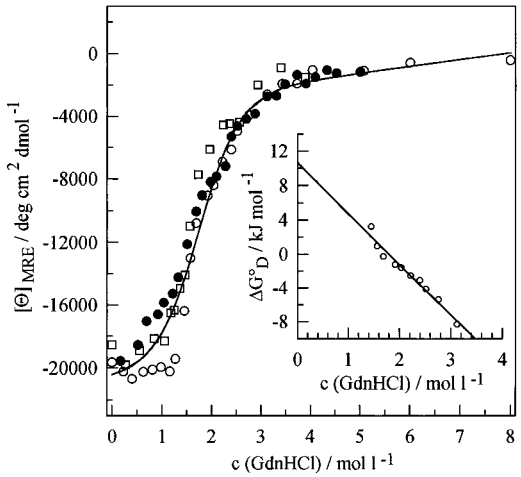

FIGURE 10: GdnHCl-induced unfolding (○) and refolding (●) curves of annexin V E17G ($c = 0.05$ mg mL^{-1}). The buffer was 50 mM Tris and 100 mM KCl, at pH 8.0 (20 °C); the mean residue ellipticity at 222 nm was calculated using a mean residue molar mass of 111.7 g mol^{-1}. Ellipticities were measured in a thermostated 1 cm cuvette and were corrected for buffer ellipticity. The guanidinium concentration was determined by refractometry using the tables of Nozaki (1972). Refolding and unfolding solutions were incubated for 24 h before CD was measured. Checks were made to ensure that equilibrium was reached after this equilibration time. The inset shows the conventional linear extrapolation of $\Delta G°_D$ that results in the same $\Delta G°_D$ (buffer) value as obtained from the two-parameter fit according to Santoro and Bolen (1988). For comparison wild-type annexin V unfolding data have been included. The corresponding measurements are labeled by open squares. Experimental conditions were identical to those of the E17G mutant.

Table 5: Characteristic Parameters Obtained from GdnHCl-Induced Un- and Refolding Studies at 20 °C in 50 mM Tris and 100 mM KCl Buffer at pH 8.0[a]

annexin V E17G	denaturation and renaturation
$c_{1/2}$ (GdnHCl) (mol L^{-1})	1.74
$\Delta G°_D$(buffer) (kJ mol^{-1})	10.4
m_G (kJ L mol^{-2})	6.0
y_N (deg cm^2 dmol^{-1})	−20220
m_N (deg cm^2 L dmol^{-1} mol^{-1})	426
y_D (deg cm^2 dmol^{-1})	−3370
m_D (deg cm^2 L dmol^{-1} mol^{-1})	426

[a] Evaluation of the transition curves was made in two ways. (a) We used the Santoro and Bolen equation (1988) as a two-parameter fit for $\Delta G°_D$ (buffer) and m_G to avoid the errors involved in a six-parameter fit. y_D, m_D, y_N, and m_N were determined independently by linear least-squares fits of the experimental pre- and posttransitional baselines. (b) Conventional evaluation of linear $\Delta G°_D$ versus [GdnHCl] plot (see the inset in Figure 10).

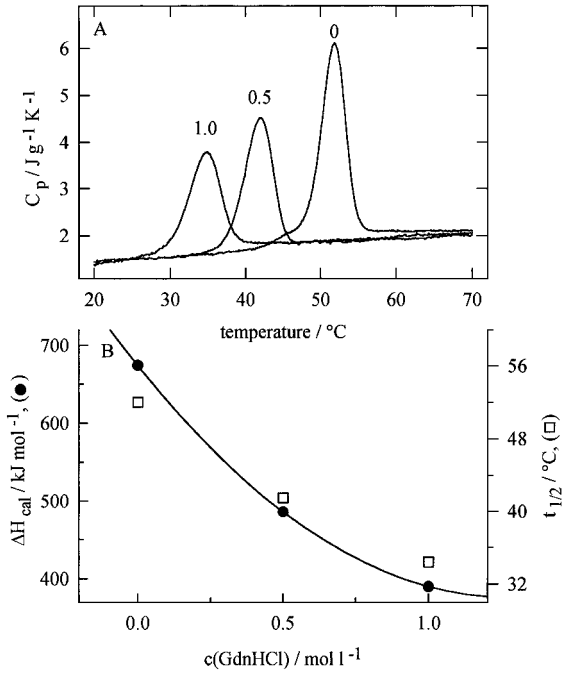

FIGURE 11: (A) Variation with GdnHCl concentration of the C_p transition curves of annexin V E17G in 50 mM Tris and 100 mM KCl at pH 8.0 (adjusted at 25 °C). The heating rate was 1 K min^{-1}. The numbers in the graph refer to the GdnHCl concentration (molar) in the solution. The transition curves in this graph have been adjusted to the same low-temperature C_p value. Therefore, they do not reflect absolute C_p values as the C_p curves in the other graphs do. (B) Illustration of the changes in transition temperature and transition enthalpy with denaturant concentration (values from Table 6).

The resulting value for ΔC_p is 32.9 kJ mol^{-1} K^{-1}, which corresponds to 103 J K^{-1} per mole of amino acid residue. Such a high heat capacity change has never been observed before, not even with highly compact proteins that have a pronounced hydrophobic core. Since annexin V E17G is neither compact nor particularly hydrophobic, we can discard the calculated ΔC_p and assume that the experimental ΔC_p value of 10.3 kJ K^{-1} mol^{-1} is correct. The difference in the $\Delta G°_D$ values from thermal and chemical unfolding reflects the fact that due to interactions with GdnHCl at low denaturant concentrations the assumption of a linear relationship between $\Delta G_{D,app}$ and the GdnHCl concentration may not be valid.

Influence of GdnHCl Concentration on the Stability of Annexin V E17G

To elucidate the differences in the stability of annexin V E17G derived from thermal and solvent-induced denaturation, we performed thermal unfolding measurements at different GdnHCl concentrations. If both $\Delta G°_D$ values from thermal and chemical unfolding are valid, the guanidinium itself must produce additional effects. Therefore, it is reasonable to expect an extraordinarily strong conformational destabilization to be associated with binding of GdnHCl to the protein. Figure 11 shows heat capacity transition curves in the presence of two GdnHCl concentrations along with a graph illustrating the dependence of both ΔH_{cal} and $t_{1/2}$ on denaturant concentration. The transition parameters in the presence of GdnHCl are summarized in Table 6.

For these measurements, we changed the buffer system from phosphate to Tris buffer (50 mM Tris-HCl and 100 mM KCl at pH 8.0 and 25 °C). The transition curves demonstrate clearly by the strong decreases in both the transition temperature (from 52.0 to 34.4 °C) and the transition enthalpy (from 674 to 390 kJ mol^{-1}) that a considerable destabilization against temperature unfolding results from the increase in the GdnHCl concentration from 0 to 1 M. Inspection of the graph implies that the decrease in ΔH_{cal} is no linear function of GdnHCl concentration although with only three points one must be careful with extrapolations.

Table 6: Thermodynamic Parameters of Annexin V E17G Unfolding at Different GdnHCl Concentrations Obtained from DSC Measurements[a]

[annexin V] (mM)	[GdnHCl] (M)	$t_{1/2}$ (°C)	ΔH_{cal} (kJ mol^{-1})	ΔH_{vH} (kJ mol^{-1})
0.0251	0	52.0 ± 0.5	674 ± 25	777 ± 15
0.0280	0.5	41.5	486	677
0.0215	1	34.4	390	589

[a] The buffer was 50 mM Tris and 100 mM KCl at pH 8.0 (25 °C); the heating rate was 1.19 K min^{-1}.

DISCUSSION

Evaluation of irreversible heat capacity measurements of proteins is an issue of fundamental significance, since it can be assumed that the majority of thermal unfolding reactions of other than small compact proteins will lack the property of reversibility. It is therefore important to delineate the constraints under which equilibrium parameters can be gleaned from apparently irreversible unfolding processes. Determination of activation properties alone is, with the exception of very simple isomerization processes, generally of minor heuristic value due to the principal difficulties involved in linking these properties to stability parameters. Unfolding of annexin V E17G affords an irreversible reaction for which it has been possible to derive equilibrium thermodynamic quantities that can be used in stability calculations. Three properties facilitated the analysis of the heat capacity curves: (a) the athermal nature of the irreversible reaction, (b) the low velocity of the first-order process that exhibits a rate constant of 1 s^{-1} (at T*) only 6−9 K above the midpoint temperature of the transition, and (c) the fact that the transition temperature becomes independent of heating rate at high scan rates. These characteristics of annexin V E17G unfolding form the basis for the simulations using eq 11 with the results shown in Figure 7.

Annexin V E17G Exhibits High Activation Energies of Unfolding but Low Specific Stability. As mentioned above, heat capacity studies on various irreversibly unfolding proteins resulted in activation energies on the order of 300 ± 100 kJ mol^{-1}. Therefore, the activation energy of annexin V E17G of about 600 kJ mol^{-1} can be considered a high value. Furthermore, it is also large in comparison to the transition enthalpy of about 680 kJ mol^{-1}. Such a high activation energy suggests that a large percentage of the native structure must be destroyed before the irreversible reaction sets in.

Annexin V E17G shows marginal stability when compared to small compact proteins. This becomes evident when the specific stability per gram of protein is calculated from the molar value of 48.3 kJ mol^{-1} by division by the molar mass. The specific stability, Δg_D, of annexin V E17G at 25 °C is

1.35 J g^{-1}, while the specific stabilities of small compact proteins at the same temperature are as follows: cytochrome *c*, Δg_D (pH 6.5) = 5.20 J g^{-1} (Knapp & Pace, 1974); tendamistat, Δg_D (pH 7) = 4.2 J g^{-1} (Renner et al., 1992); lysozyme, Δg_D (pH 7) = 4.25 J g^{-1} (Privalov & Khechinashvili, 1974); metmyoglobin, Δg_D (pH 7) = 2.76 J g^{-1} (Puett, 1973); and RNase, Δg_D (pH 7) = 4.28 J g^{-1} (Tsong et al., 1970).

Despite this marginal stability, tertiary interactions between the various structural modules appear to be sufficiently strong to prevent decoupling of, for example, those domains which are known to be involved in hinge bending motions. If coupling did not exist, one would expect that the overall transition curve could be deconvolved into two-state subtransitions corresponding to the uncoupled domains. If that were the case, we should under equilibrium conditions observe smaller values for the van't Hoff enthalpies than for the calorimetric enthalpies. The actual finding is just the opposite. All van't Hoff values found were larger than or equal to the calorimetric enthalpies. Therefore, there is no indication that would suggest that in general discrete domain unfolding occurs but is masked by the structural similarity of the discrete components.

The small value of the heat capacity change, ΔC_p, associated with unfolding is also in line with the low conformational stability. It implies that changes in the exposure to solvent on unfolding are smaller than for proteins having sequestered hydrophobic cores or, in other words, that annexin V E17G is already rather well solvated in its native conformation. This idea is consistent with the structural features of annexin V E17G that are characterized by mobility of domains and formation of pores. The latter property could be associated with facilitated access of water to the pore-forming surface and thereby increase the native state hydration.

A very surprising result of the present studies is the large apparent discrepancy between the Gibbs energy values obtained from thermal and GdnHCl-induced unfolding. Generally, there had been fairly good, though seldom perfect, agreement between the stability parameters obtained from heat capacity and denaturant studies (Pace et al., 1991; Steif et al., 1993). The differences could be assigned to uncertainties in the ΔC_p determination of the DSC measurements or to problems involved in the linear extrapolation of the $\Delta G°_{app}$ values to zero denaturant concentration for systems having very high $c_{1/2}$ values for the denaturant. However, the difference between $\Delta G°_D$ (20 °C) = 53.4 kJ mol^{-1} derived from DSC studies and $\Delta G°_D$ (buffer, 20 °C) = 10.4 kJ mol^{-1} obtained from the GdnHCl unfolding of annexin V E17G is too large to rationalize by small errors errors associated with the heat capacity change or with the slope of the linear $\Delta G_{D,app}$ versus *T* curve. Rather, we have to consider this discrepancy an indication of the occurrence of different mechanisms of unfolding in the thermal and chemical denaturation which does not permit us to use a linear plot in the determination of ΔG_D (buffer) from the GdnHCl unfolding studies.

There is support for this assumption from the low GdnHCl midpoint concentration, $c_{1/2}$ = 1.74 M, of the isothermal transition curve and, particularly, from the unusually large decrease in the transition temperature $\Delta t_{1/2}$ (=18 °C) that results from an increase in GdnHCl concentration by 1 M (Figure 11). Generally, the observed changes are within $\Delta t_{1/2}$ = 8 ± 2 °C per 1 M change in GdnHCl concentration (Litvinovich et al., 1991; Steif et al., 1993; Pace et al., 1991). Furthermore, the decrease in ΔH_{cal} in the presence of GdnHCl appears to be a nonlinear function of denaturant concentration, where small GdnHCl concentrations have relatively strong effects. This can be interpreted as being indicative of an unusual perturbation in the interactions of annexin V E17G by GdnHCl, provided one assumes that the regular mechanism of structure destabilization by GdnHCl, as observed for a series of proteins, is associated with the smaller decrease of $t_{1/2}$ as mentioned before.

It is the combination of both a low $c_{1/2}$ value and slope that results in the extraordinarily small extrapolated $\Delta G°_D$ (buffer) value for annexin V E17G. A nonlinear increase in slope with decreasing GdnHCl concentration would of course remove the disparity between the stability parameters. There are proteins that show low $c_{1/2}$ values and others with small slopes in the $\Delta G°_{app}$ versus [GdnHCl] plots, but so far as we know, coincidence of small values of both quantities has not been observed (Myers et al., 1995). For example, Lys25-RNase T1 exhibits a small slope in the $\Delta G°_{app}$ versus [GdnHCl] plot, but it has a $c_{1/2}$ value of 3.7 M (Kiefhaber et al., 1990). Therefore, the extrapolation yields a regular stability value. On the other hand, DsbA shows a $c_{1/2}$ value as low as that of annexin which is, however, linked to a slope, *m*, 5 times higher than that observed with annexin V E17G (Wunderlich et al., 1993).

The small m_G value of 6000 J mol^{-1} M^{-1} observed for annexin V E17G is consistent with the small value for ΔC_p, as has been recently shown by Myers et al. (1995) in an extensive survey on the correlations between m_G values, heat capacity changes, and changes in accessible surface area. This is further support for the assumption that the low experimental ΔC_p value of annexin V is indeed characteristic of the conformational change of the protein and not an artifact of the irreversibility of the unfolding reaction. We consider these findings supportive evidence for an unusual interaction of annexin V E17G with GdnHCl that precludes derivation of the overall intrinsic stability from the conventional linear extrapolation of the apparent Gibbs energy of chemical denaturation to zero denaturant concentration. The mechanism of this interaction will be the subject of further investigations.

REFERENCES

Ahn, G. N., Teller, D. C., Bienkowski, M. J., McMullen, B. A., Lipkin, E. W., & de Haen, C. (1988) *J. Biol. Chem. 263*, 18657−18663.

Andree, H. A. M., Stuart, M. C. A., Hermens, W. Th., Reutelingsperger, C. P. M., Hemker, H. C., Frederik, P. M., & Willems, G. M. (1992) *J. Biol. Chem. 267*, 17907−17912.

Andree, H. A. M., Willems, G. M., Hauptmann, R., Maurer-Fogy, I., Stuart, M. C. A., Hermens, W. T., Frederik, P. M., & Reutelingsperger, C. P. M. (1993) *Biochemistry 32*, 4634−4640.

Bazzi, M. D., & Nelsestuen, G. L. (1992) *Biochemistry 31*, 10406−10413.

Berendes, R., Voges, D., Demange, P., Huber, R., & Burger, A. (1993) *Science 262*, 427−430.

Bewley, M. C., Boustead, C. M., Walker, J. H., Waller, D. A., & Huber, R. (1993) *Biochemistry 32*, 3923−3929.

Blackwood, R. A., & Ernst, J. D. (1990) *Biochem. J. 266*, 195−200.

Brisson, A., Mosser, G., & Huber, R. (1991) *J. Mol. Biol. 220*, 199−203.

Burger, A., Voges, D., Demange, P., Perez, C. R., Huber, R., & Berendes, R. (1994) *J. Mol. Biol. 237*, 479−499.

Concha, N. O., Head, J. F., Kaetzel, M. A., Dedman, J. R., & Seaton, B. A. (1993) *Science 261*, 1321−1324.
Conejero-Lara, F., Sanchez-Ruiz, J. M., Mateo, P. L., Burgos, F. J., Vendrell, J., & Aviles, F. X. (1991a) *Eur. J. Biochem. 200*, 663−670.
Conejero-Lara, F., Mateo, P. L., Aviles, F. X., & Sanchez-Ruiz, J. M. (1991b) *Biochemistry 30*, 2067−2072.
Creutz, C. E. (1992) *Science 258*, 924−931.
Demange, P., Voges, D., Benz, J., Liemann, S., Göttig, P., Berendes, R., Burger, A., & Huber, R. (1994) *Trends Biochem. Sci. 7*, 272−277.
Freire, E., van Osdol, W. W., Mayorga, O. L., & Sanchez-Ruiz, J. M. (1990) *Annu. Rev. Biophys. Biophys. Chem. 19*, 159−188.
Funakoshi, T., Heimark, R. L., Hendrickson, L. E., McMullen, B. A. Fujikawa, K. (1987) *Biochemistry 26*, 5572−5578.
Galisteo, M. L., & Sanchez-Ruiz, J. M. (1993) *Eur. Biophys. J. 22*, 25−30.
Galisteo, M. L., Mateo, P. L., & Sanchez-Ruiz, J. M. (1991) *Biochemistry 30*, 2061−2066.
Gerstein, M., Lesk, A. M., & Chothia, C. (1994) *Biochemistry 33*, 6739−6749.
Giambanco, I., Verzini, M., & Donato, R. (1993) *Biochem. Biophys. Res. Commun. 196*, 1221−1226.
Gill, S. C., & von Hippel, P. H. (1989) *Anal. Biochem. 182*, 319−326.
Gilmanshin, R., Creutz, C. E., & Tamm, L. K. (1994) *Biochemistry 33*, 8225−8232.
Griko, Y. V., & Privalov, P. L. (1992) *Biochemistry 31*, 8810−8815.
Grundman, U., Abel, K.-J., Bohn, H., Löbermann, H., Lottspeich, F., & Küpper, H. (1988) *Proc. Natl. Acad. Sci. U.S.A. 85*, 3708−3712.
Guzmán-Casado, M., Parody-Morreale, A., Mateo, P. L., & Sanchez-Ruiz, J. M. (1990) *Eur. J. Biochem. 188*, 181−185.
Huber, R., Römisch, J., & Paques, E.-P. (1990a) *EMBO J. 9*, 3867−3874.
Huber, R., Schneider, M., Mayr, I., Römisch, J., & Paques, E.-P. (1990b) *FEBS Lett. 275*, 15−21.
Huber, R., Berendes, R., Burger, A., Schneider, M., Karshikov, A., Luecke, H., Römisch, J., & Paques, E. (1992) *J. Mol. Biol. 223*, 683−704.
Johnstone, S. A., Hubaishy, I., & Waisman, D. M. (1992) *J. Biol. Chem. 267*, 25976−25981.
Junker, M., & Creutz, C. E. (1993) *Biochemistry 32*, 9968−9974.
Karshikov, A., Berendes, R., Burger, A., Cavalié, A., Lux, H.-D., & Huber, R. (1992) *Eur. Biophys. J. 20*, 337−344.
Kiefhaber, T., Schmid, F. X., Renner, M., Hinz, H.-J., Hahn, U., & Quaas, R. (1990) *Biochemistry 29*, 8250−8257.
Knapp, J. A., & Pace, N. (1974) *Biochemistry 13*, 1289−1294.
Lewitt-Bentley, A., Morera, S., Huber, R., & Bodo, G. (1992) *Eur. J. Biochem. 210*, 73−77.
Lewitt-Bentley, A., Bentley, G. A., Favier, B., L'Hermite, G., & Renouard, M. (1994) *FEBS Lett. 345*, 38−42.
Litvinovich, S. V., Strickland, D. K., Medved, L. V., & Ingham, K. C. (1991) *J. Mol. Biol. 217*, 563−575.
Lumry, R., & Eyring, H. (1954) *J. Phys. Chem. 58*, 110−120.
Meers, P. (1990) *Biochemistry 29*, 3325−3330.
Meers, P., & Mealy, T. (1993a) *Biochemistry 32*, 11711−11721.
Meers, P., & Mealy, T. (1993b) *Biochemistry 32*, 5411−5418.
Meers, P., & Mealy, T. (1994) *Biochemistry 33*, 5829−5837.
Mosser, G., Ravanat, C., Freyssinet, J.-M., & Brisson, A. (1991) *J. Mol. Biol. 217*, 241−245.
Murphy, K. P., Bhakuni, V., Xie, D., & Freire, E. (1992) *J. Mol. Biol. 227*, 293−306.
Myers, J. K., Pace, C. N., & Scholtz, J. M. (1995) *Protein Sci. 4*, 2138−2148.
Neumann, J.-M., Sanson, A., & Lewitt-Bentley, A. (1994) *Eur. J. Biochem. 225*, 819−825.
Novokhatny, V. V., Kudinov, S. A., & Privalov, P. L. (1984) *J. Mol. Biol. 179*, 215−232.
Nozaki, Y. (1972) *Methods Enzymol. 26*, 43−50.
Oobatake, M., & Ooi, T. (1993) *Prog. Biophys. Mol. Biol. 59*, 237−284
Pace, C. N., Heinemann, U., Hahn, U., & Saenger, W. (1991) *Angew. Chem. 103*, 351−369.
Pantoliano, M. W., Whitlow, M., Wood, J. F., Dodd, S. W., Hardman, K. D., Rollence, M. L., & Bryan, P. N. (1989) *Biochemistry 28*, 7205−7213.
Perkins, S. J. (1986) *Eur. J. Biochem. 157*, 169−180.
Pigault, C., Follenius-Wund, A., Schmutz, M., Freyssinet, J.-M., & Brisson, A. (1994) *J. Mol. Biol. 236*, 199−208.
Pollard, H. B., & Rojas, E. (1988) *Proc. Natl. Acad. Sci. U.S.A. 85*, 2974−2978.
Privalov, P. L. (1980) *Pure Appl. Chem. 52*, 479−497.
Privalov, P. L., & Khechinashvili, N. N. (1974) *J. Mol. Biol. 86*, 665−684.
Puett, D. (1973) *J. Biol. Chem. 248*, 4623−4634.
Ragone, R., & Colonna, G. (1994) *Biochim. Biophys. Acta 1208*, 15−21.
Ramsay, G., & Freire, E. (1990) *Biochemistry 29*, 8677−8683.
Renner, M., Hinz, H.-J., Scharf, M., & Engels, J. W. (1992) *J. Mol. Biol. 223*, 769−779.
Ross, T. S., Tait, J. F., & Majerus, P. W. (1990) *Science 248*, 605−607.
Sanchez-Ruiz, J. M. (1992) *Biophys. J. 61*, 921−935.
Sanchez-Ruiz, J. M., López-Lacomba, J. L., Cortijo, M., & Mateo, P. L. (1988) *Biochemistry 27*, 1648−1652.
Santoro, M. M., & Bolen, D. W. (1988) *Biochemistry 27*, 8063−8068.
Schmid, F. X. (1989) Spectral methods of characterizing protein conformation and conformational changes, *Protein Structure- a practical Approach* (Creighton, T. E., Ed.) pp 251−285, IRL Press at Oxford University Press, Oxford.
Sopkova, J., Renouard, M., & Lewit-Bentley, A. (1993) *J. Mol. Biol. 234*, 816−825.
Sopkova, J., Gallay, J., Vincent, M., Pancoska, P., & Lewit-Bentley, A. (1994) *Biochemistry 33*, 4490−4499.
Steif, C., Weber, P., Hinz, H.-J., Flossdorf, J., Cesareni, G., & Kokkinidis, M. (1993) *Biochemistry 32*, 3867−3876.
Tsong, T. Y., Hearn, R. P., Wrathall, D. P., & Sturtevant, J. M. (1970) *Biochemistry 9*, 2666−2677.
Voges, D., Berendes, R., Burger, A., Demange, P., Baumeister, W., & Huber, R. (1994) *J. Mol. Biol. 238*, 199−213.
Wunderlich, M., Jaenicke, R., & Glockshuber, R. (1993) *J. Mol. Biol. 233*, 559−566.
Yang, J. T., Wu, C.-S. C., & Martinez, H. M. (1986) *Methods Enzymol. 130*, 208−269.

BI962163Z